

1 Title

2

3 **Eddy Covariance Evaluation of Ecosystem Fluxes at a Temperate Saltmarsh in**  
4 **Victoria, Australia Shows Large CO<sub>2</sub> Uptake**

5

6 Authors

7

8 Ruth Reef<sup>1</sup>,

9 Edoardo Daly<sup>2,3</sup>,

10 Tivanka Anandappa<sup>1</sup>,

11 Eboni-Jane Vienna-Hallam<sup>1</sup>,

12 Harriet Robertson<sup>1</sup>,

13 Matthew Peck<sup>1</sup>,

14 Adrien Guyot<sup>4,5</sup>

15

16 Affiliations

17

18 1 School of Earth, Atmosphere and Environment, Monash University, VIC 3800, Australia

19 2 Department of Civil Engineering, Monash University, VIC 3800, Australia

20 3 WMAwater, Brisbane, QLD 4000, Australia

21 4 Atmospheric Observations Research Group, The University of Queensland, Brisbane,

22 Australia

23 5 Australian Bureau of Meteorology, Melbourne, Australia

24

25 Corresponding Author

26

27 Associate Professor Ruth Reef

28 School of Earth Atmosphere and Environment

29 Monash University

30 9 Rainforest Walk, Clayton VIC 3800

31 Australia

32 Email: [ruth.reef@monash.edu](mailto:ruth.reef@monash.edu)

33 Ph: +61 3 9905 8309

34

35

36 Key Points

37

38 This is the first study using eddy covariance to measure CO<sub>2</sub> fluxes at an Australian  
39 temperate saltmarsh, revealing temperature and light limitations to CO<sub>2</sub> uptake.

40

41 CO<sub>2</sub> fluxes varied seasonally; growing season net ecosystem productivity was 10.54 g CO<sub>2</sub>  
42 m<sup>-2</sup> day<sup>-1</sup>, dropping to 1.64 g CO<sub>2</sub> m<sup>-2</sup> day<sup>-1</sup> in winter.

43

44 Productivity at the French Island saltmarsh is high relative to global saltmarsh estimates but  
45 below global mangrove averages.

46

47

48

49 Abstract

50

51 Recent studies highlight the important role of vegetated coastal ecosystems in atmospheric  
52 carbon sequestration. Saltmarshes constitute 30% of these ecosystems globally and are the  
53 primary intertidal coastal wetland habitat outside the tropics. Eddy covariance (EC) is the  
54 main method for measuring biosphere-atmosphere fluxes, but its use in coastal environments  
55 is rare. At an Australian temperate saltmarsh site on French Island, Victoria, we measured  
56 CO<sub>2</sub> and water gas concentration gradients, temperature, wind speed and radiation. The  
57 marsh was dominated by a dense cover of *Sarcocornia quinqueflora*. Fluxes were seasonal,  
58 with minima in winter when vegetation is dormant. Net ecosystem productivity (NEP) during  
59 the growing season averaged 10.54 g CO<sub>2</sub> m<sup>-2</sup> day<sup>-1</sup> decreasing to 1.64 g CO<sub>2</sub> m<sup>-2</sup> day<sup>-1</sup> in  
60 the dormant period, yet the marsh remained a CO<sub>2</sub> sink due to some sempervirent species.  
61 Ecosystem respiration rates were lower during the dormant period compared with the  
62 growing season (1.00 vs 1.77 μmol CO<sub>2</sub> m<sup>-2</sup> s<sup>-1</sup>) with a slight positive relationship with  
63 temperature. During the growing season, fluxes were significantly influenced by light levels,  
64 ambient temperatures and humidity with cool temperatures and cloud cover limiting NEP.  
65 Ecosystem water use efficiency of 0.86 g C kg<sup>-1</sup> H<sub>2</sub>O was similar to other C3 intertidal  
66 marshes and evapotranspiration averaged 2.48 mm day<sup>-1</sup> during the growing season.

67

68 EGUsphere Topics

69 Emissions, Marine and Freshwater Biogeosciences, Earth System Biogeosciences

70

71 Short Summary

72

73 Studies show that saltmarshes excel at capturing carbon from the atmosphere. In this study,  
74 we measured CO<sub>2</sub> flux in an Australian temperate saltmarsh on French Island. The temperate  
75 saltmarsh exhibited strong seasonality. During the warmer growing season, the saltmarsh  
76 absorbed on average 10.5 grams of CO<sub>2</sub> from the atmosphere per m<sup>2</sup> daily. Even in winter,  
77 when plants were dormant, it continued to be a CO<sub>2</sub> sink, albeit smaller. Cool temperatures  
78 and high cloud cover inhibit carbon sequestration.

79

80

81

82

83 1. Introduction

84

85 Despite their relatively small global footprint of 54,650 km<sup>2</sup> (Mcowen et al., 2017), salt  
86 marshes provide a range of ecosystem services, including shoreline protection (Shepard et al.,  
87 2011), nutrient uptake, nursery grounds for fish populations (Whitfield, 2017) as well as  
88 functioning as significant carbon sinks through CO<sub>2</sub> uptake and storage in their organic rich  
89 sediments (McLeod et al., 2011). These ‘blue carbon’ habitats are recognised for their  
90 significant contribution to the global carbon cycle, as coastal wetlands more broadly are  
91 estimated to have accumulated more than a quarter of global organic soil carbon (Duarte,  
92 2017).

93

94 Saltmarshes are a widely distributed intertidal habitat but are floristically divergent globally  
95 (Adam, 2002), such that commonalities in function and form do not extend across  
96 biogeographic realms. US saltmarshes, for example, are extensively dominated by a single  
97 grassy species, *Spartina alterniflora*, as opposed to the dominance of C<sub>3</sub> Chenopodioideae  
98 species in the southern hemisphere (Adam, 2002). Temperate saltmarshes occupy a  
99 latitudinal range spanning from approximately 30° to 60° (Mcowen et al., 2017) and are most  
100 commonly found along protected coastlines such as bays, estuaries, and lagoons, where they  
101 are sheltered from the full force of wave action (Mitsch and Gosselink, 2000). In the  
102 Southern Hemisphere, temperate saltmarshes have a strong Gondwanan element with high  
103 floristic similarity among the marshes of New Zealand, the southernmost coasts of South  
104 America and South Africa and the southern coastlines of Australia (Adam, 1990). These  
105 marshes are often associated with extensive seagrass meadows and mudflats, and in parts of  
106 their range, mangroves, forming complex coastal mosaics (Huxham et al., 2018).  
107 Saltmarshes have been heavily degraded across their range, and it is estimated that perhaps  
108 up to 50% of the global saltmarsh area has been lost since 1900 (Gedan et al., 2009),  
109 primarily due to land use change.

110

111 In most areas where they occur, seasonality plays a major role in the functioning of temperate  
112 saltmarshes (Ghosh and Mishra, 2017). These ecosystems experience distinct growing and  
113 dormant seasons, primarily driven by temperature, light availability, and precipitation  
114 patterns (Adam, 2000). During the growing season (typically spring and summer), increased  
115 temperatures and longer daylight hours stimulate plant growth, photosynthetic activity, and

116 decomposition processes. Photosynthesis typically outpaces decomposition during this  
117 period, resulting in the temperate saltmarsh acting as a net CO<sub>2</sub> sink (Chmura et al., 2003).  
118 Conversely, the dormant season (usually fall and winter) is characterized by cooler  
119 temperatures and shorter days (Adam, 2000; Howe et al., 2010). These factors lead to  
120 reduced plant growth and photosynthetic activity (Adam, 2000) and while decomposition  
121 processes also slow down due to cooler temperatures, CO<sub>2</sub> release through decomposition  
122 often exceeds CO<sub>2</sub> uptake during this period (Artigas et al., 2015). In Australia, saltmarshes  
123 have been assumed to not exhibit seasonality (Owers et al., 2018) despite there being a  
124 scarcity of data on saltmarsh phenology and the implication this untested assumption could  
125 have on carbon budget estimations.

126  
127 Gross primary production (GPP) of saltmarshes is the total amount of CO<sub>2</sub> uptake by plants  
128 through photosynthesis. Respiration (R<sub>c</sub>) leads to a CO<sub>2</sub> flux directed back to the atmosphere  
129 due to all respiration processes occurring within the saltmarsh, involving both autotrophs and  
130 heterotrophs. The difference between these two fluxes is the net ecosystem exchange (NEE).  
131 Saltmarsh ecosystems can act as both sources and sinks of carbon dioxide (CO<sub>2</sub>), influencing  
132 atmospheric CO<sub>2</sub> concentrations (Chmura et al., 2003). However, quantifying their net  
133 exchange remains challenging (Lu et al., 2017) hindering their effective inclusion in Earth  
134 System Models (Ward et al., 2020) and confounding the incorporation of saltmarsh  
135 restoration in emission reduction targets. Eddy covariance (EC) provides a powerful method  
136 for near-continuous, high-frequency monitoring of gas exchange between a vegetated surface  
137 and the atmosphere (Baldocchi, 2003), enabling the determination of net ecosystem exchange  
138 (NEE) of CO<sub>2</sub>, and identifying the forcings that determine how CO<sub>2</sub> fluxes will respond to  
139 global climate change (Borges et al., 2006; Cai, 2011).

140  
141 Previous EC studies in coastal saltmarshes have been focused on the Northern Hemisphere, in  
142 sites in the USA (e.g. Hill and Vargas, 2022; Kathilankal et al., 2008; Moffett et al., 2010;  
143 Nahrawi et al., 2020; Schäfer et al., 2019), France (Mayen et al., 2024), Japan (Otani and  
144 Endo, 2019) and China (Wei et al., 2020) but interest in the southern hemisphere is growing  
145 (Bautista et al., 2023). The NEE values from these studies indicate that there is high inter-site  
146 (as well as interannual, Erickson et al., (2013)) variability in carbon dynamics of saltmarshes,  
147 with a link to species types, salinity, hydrology (Moffett et al., 2010; Nahrawi et al., 2020),  
148 site specific biochemical conditions (Seyfferth et al., 2020) and latitude (Feagin et al., 2020).  
149 While generally considered important carbon sinks (e.g. ranging between 130 to 775 g C m<sup>-2</sup>

150 yr<sup>-1</sup> in the USA, according to Kathilankal et al. (2008) and Wang et al.(2016) respectively)  
151 and globally hypothesised to average 382 g C m<sup>-2</sup> y<sup>-1</sup> (Alongi, 2020), some EC studies  
152 revealed saltmarshes to be net sources of CO<sub>2</sub> to the atmosphere (Vázquez-Lule and Vargas,  
153 2021) especially in temperate saltmarshes that experience long dormant periods.

154  
155 The aim of this study is to estimate CO<sub>2</sub> and water fluxes in a temperate saltmarsh in  
156 Victoria, southern Australia, to better characterise the effect of seasonality and environmental  
157 variables on the saltmarsh CO<sub>2</sub> budgets. This is the first study in an Australian coastal  
158 saltmarsh where CO<sub>2</sub> fluxes are estimated using the EC method.

159

## 160 2. Methods

161

### 162 2.1 Site Description

163

164 Ecosystem flux measurements were collected at the Tortoise Head Ramsar coastal wetland on  
165 French Island, Victoria (38.388°S, 145.278°E, Fig. 1) within the Western Port embayment.

166 French Island is within the Cfb climate zone (temperate oceanic climate) and experiences  
167 distinct seasonal variations in temperature and precipitation. Long term (30 year) climate data  
168 averaged from the nearby Cerberus Station (Australian Bureau of Meteorology, site 86361)  
169 indicated that summers, spanning from December through February, are generally mild to  
170 warm, with maximum temperatures typically ranging from 17°C to 25°C although occasional  
171 heatwaves lead to temporary spikes in temperature that can exceed 30°C. Winters, from June  
172 to September, are cooler, with maximum temperatures ranging between 7°C and 14°C and a  
173 mean minimum temperature of 6°C. Frost is infrequent due to maritime influence, though  
174 crisp mornings below 0°C occur 10% of the time in winter. Rainfall, evenly distributed

175 throughout the year, averages ca. 715 mm y<sup>-1</sup>, although in 2020 the site ~~had higher than~~  
176 average rainfall (860 mm y<sup>-1</sup>). The island is exposed to weather patterns influenced by the  
177 Southern Ocean and Bass Strait, leading to occasional storm systems, particularly in winter,  
178 bringing gusty winds and increased precipitation. Western Port has semi-diurnal tides with a  
179 range of nearly 3 m, resulting in wide intertidal flats occupied by mangroves of the species

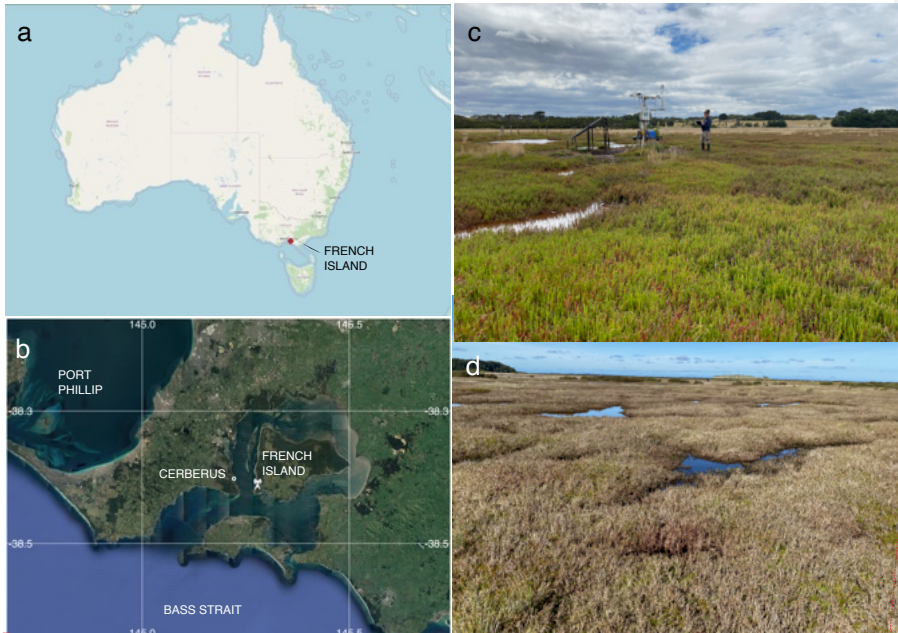
180 *Avicennia marina* and saltmarshes. The saltmarsh in this study experiences complex

181 hydrological conditions, and we found that inundation does not directly link to tides.

182

Formatted: Outline numbered + Level: 2 + Numbering  
Style: 1, 2, 3, ... + Start at: 1 + Alignment: Left + Aligned at:  
0.63 cm + Indent at: 1.27 cm

Deleted: led



184

185

186 Figure 1: a) The location of French Island along the Bass Strait coast of Australia, and b) The  
 187 location of the flux tower on French Island as well as the nearby Cerberus meteorological  
 188 station (Bureau of Meteorology, Australia), © Google Earth. c) An image of the saltmarsh  
 189 within the flux tower footprint during the growing season (with the tower and the author in  
 190 the background), taken in February 2020 by Prudence Perry. d) an image of the saltmarsh  
 191 during the dormant period, taken at the same location in September 2020 by Ruth Reef.

192

193 The site at French Island is dominated by an extensive temperate coastal saltmarsh  
 194 community that is a particularly good natural representation of a broader biogeographic  
 195 saltmarsh grouping which covers an area of ca. 7000 ha along Victoria's central coast  
 196 embayments (Navarro et al., 2021). While the wetland at the site is a saltmarsh-mangrove-  
 197 seagrass wetland system, the footprint of the flux tower was limited to the saltmarsh alone,  
 198 which extends more than a kilometre from the shoreline in places. This geography provided  
 199 the critical horizontally homogenous area with flat terrain required for ecosystem flux  
 200 measurements. Floristically this saltmarsh is species poor, dominated by *Sarcocornia*  
 201 *quinqueflora*. Stands of *Tecticornia arbuscula* are common in this saltmarsh, while *Atriplex*

203 *cinerea* and *Sarcocornia quinqueflora* and *Distichis distichophylla* can be prevalent depending on  
204 elevation and soil drainage conditions. *Sarcocornia quinqueflora* is a perennial succulent and  
205 at the temperate ranges of its distribution it has a distinct growing season from October to  
206 May (Fig. 1c) when the stems turn red, followed by a woody and fibrous dormant period  
207 during the colder months of June through September (Fig. 1d). The height of the dominant  
208 vegetation ranged between 0.3 m.

209

## 210 2.2 Data Collection and Analysis

211

212 Eddy covariance measurements were made between November 2019 and August 2021  
213 capturing both the saltmarsh growing season (October-May) as well as a dormant period  
214 (June-September). An array of standard micro-meteorological instruments included a 3-  
215 dimensional sonic anemometer (CSAT3, Campbell Scientific, USA), an open-path infra-red  
216 carbon dioxide (CO<sub>2</sub>) gas and water vapour (H<sub>2</sub>O) analyser (Li-7500, Li-Cor, USA) and 2  
217 data-loggers. The tower was powered by a solar array with two accompanying 12V DC  
218 storage batteries. The sonic anemometer was mounted 2.3 m above ground. The CO<sub>2</sub>/H<sub>2</sub>O  
219 gas analyser was mounted 0.11 m longitudinally displaced from the anemometer. A CR3000  
220 datalogger (Campbell Scientific, USA), recorded the Li-7500, anemometer, short- and long-  
221 wave radiation (CNR4, Klip & Zonen, the Netherlands), air temperature and humidity (083E,  
222 Met One, USA) readings at 10 Hz frequency. Due to the location of the site in the Bass Strait  
223 (a region that experiences regular winter storms, high wind speeds and higher than national  
224 average cloud cover) the tower sustained damage due to winter storms several times during  
225 the deployment, as well as suffered periods of poor power supply due to short day lengths  
226 and high cloud cover; this was exacerbated by poor accessibility to the remote location during  
227 COVID-19 travel restrictions. The analysis thus focused on extended periods of continuous  
228 daily records and periods with large gaps in the dataset were removed.

229

230 Ecosystem fluxes were calculated for 30 min intervals using Eddy Pro software v.7 (LI-COR  
231 Inc., USA) Express Mode protocols (see settings at  
232 <https://www.licor.com/env/support/EddyPro/topics/express-defaults.html>). This processing  
233 step includes coordinate axis rotation correction, trend correction, data synchronisation,  
234 statistical tests for quality, density corrections and spectrum corrections. As part of this step,  
235 flux quality flags were assigned to the calculated CO<sub>2</sub> fluxes using the 0–2 flag policy

Deleted: 2.2

Formatted: Outline numbered + Level: 2 + Numbering  
Style: 1, 2, 3, ... + Start at: 1 + Alignment: Left + Aligned at:  
0.63 cm + Indent at: 1.27 cm

Deleted: .



238 ‘Mauder and Foken 2004’, based on the steady state test and the developed turbulent  
 239 conditions test. The steady state test checks if fluxes remain consistent over the 30-minute  
 240 averaging period by comparing the mean and standard deviation (SD) of fluxes in the first  
 241 and second halves of the period. The developed turbulent conditions test ensures turbulence is  
 242 well-developed and its energy spectra fits the Kolmogorov spectrum. Both tests assign partial  
 243 flags that are combined into a single flag (0–2) in Eddy Pro, indicating the overall data  
 244 quality. Only data that met the criteria of being in quality class 0 (‘best quality fluxes’) for  
 245 CO<sub>2</sub> flux were chosen for further analysis. We further removed anomalous data points  
 246 defined as values that exceed four SDs from the mean CO<sub>2</sub> flux; this resulted in the additional  
 247 loss of ca. 1% of the dataset. Gap filling was not applied. Additional filtering was applied to  
 248 nighttime data due to known weak convection at night, thus CO<sub>2</sub> flux data during periods of  
 249 atmospheric stability, i.e. when night friction wind velocities ( $u^*$ ) were below 0.2 m s<sup>-1</sup>, were  
 250 excluded following inspection of the nightly NEE vs.  $u^*$  curve to detect the threshold where  
 251 NEE fall-off occurs (i.e. the [Change Point Detection method, Barr et al., 2013](#)). This resulted  
 252 in a dataset of 674 day-time and 606 nighttime flux measurements during the dormant period  
 253 and 4124 day-time and 3020 nighttime flux measurements for the growing period (Table 1).  
 254 The growing season dataset included 90 days with 85% or more flux data coverage, while the  
 255 dormant season dataset included 18 days, and these days were used for 24-hour flux  
 256 integrations.

257  
 258 Table 1: Mean ( $\pm$ SD) net ecosystem exchange ( $\mu\text{mol CO}_2 \text{ m}^{-2} \text{ s}^{-1}$ ) during day- and nighttime  
 259 respectively, as well as the corresponding number of half hourly measurements from each  
 260 month, following filter applications (n).  
 261

Month	Daytime Mean NEE (SD); n	Nighttime Mean NEE (SD); n	Season
October 2019	-2.29 (3.08); 121	2.04 (1.28); 70	Greening up
November 2019	-1.84 (3.89); 151	2.85 (1.75); 110	Greening up
December 2019	-3.33 (4.59); 96	1.14 (1.70); 15	Growing
January 2020	-1.31 (3.31); 63	2.10 (0.79); 27	Growing
February 2020	-3.83 (4.11); 540	1.89 (1.10); 280	Growing
March 2020	-3.86 (3.90); 494	1.63 (0.78); 351	Growing
August 2020	0.05 (2.05); 150	1.76 (1.22); 39	Dormant
September 2020	-0.98 (2.04); 147	1.27 (0.96); 101	Dormant
January 2021	-4.81 (5.04); 602	2.15 (1.55); 373	Growing
February 2021	-3.62 (4.27); 615	2.00 (1.19); 423	Growing

Deleted: . 0.2 m s<sup>-1</sup> is

Deleted: typical threshold value used in eddy-covariance studies (Davis

Deleted: 2003

Deleted: Pink shading indicates the dormant season at the French Island saltmarsh.

Inserted Cells

Formatted Table

March 2021	-3.07 (3.95); 660	1.76 (1.20); 556	<u>Growing</u>
April 2021	-2.08 (3.02); 409	1.15 (0.87); 403	<u>Growing</u>
May 2021	-0.98 (2.57); 377	1.14 (1.04); 423	<u>End of Growing</u>
June 2021	0.58 (1.67); 271	0.93 (1.30); 328	<u>Dormant</u>
July 2021	1.07 (1.38); 102	0.82 (0.62); 127	<u>Dormant</u>

268

269

270 Half-hourly average CO<sub>2</sub> flux was measured in μmol m<sup>-2</sup> s<sup>-1</sup>, with positive fluxes indicating a  
 271 flux direction from the Earth's surface to the atmosphere. Net ecosystem exchange (NEE)  
 272 was defined as the net flux of CO<sub>2</sub> from the atmosphere to the marsh and was often negative  
 273 during daytime, indicating that Gross Primary Productivity (GPP) was larger than ecosystem  
 274 respiration (R<sub>e</sub>). Evapotranspiration (ET) was calculated by Eddy Pro as the ratio between the  
 275 latent heat flux (LE) and latent heat of vaporisation (λ). Ecosystem water use efficiency  
 276 (WUE<sub>e</sub>) was then expressed as the ratio between daytime net ecosystem productivity in g  
 277 CO<sub>2</sub> m<sup>-2</sup> h<sup>-1</sup> and evapotranspiration in mm h<sup>-1</sup>.

278

279 A two-dimensional footprint estimation was provided according to the simple footprint  
 280 parameterisation described in Kljun et al. (2015) calculating the ground position of the  
 281 cumulative fraction of flux source contribution by distance for each 30-minute interval. We  
 282 assessed the short-term effects of environmental factors on CO<sub>2</sub> fluxes at a half-hourly time  
 283 scale (e.g. the effects of light, air temperature and vapour pressure deficit) using a series of  
 284 non-linear or linear models. These analyses were limited to the growing season, when the  
 285 plants were actively photosynthesising. To calculate the daily-integrated CO<sub>2</sub> and H<sub>2</sub>O fluxes,  
 286 the daily sum of these fluxes was determined for days with at least 85% data coverage. This  
 287 involved using the trapezoid rule to estimate the area under the curve for each of these 24-  
 288 hour periods. The trapezoid rule approximates the total flux by dividing the day into smaller  
 289 intervals, each lasting 1,800 seconds (30 minutes). For each data interval, the area is  
 290 calculated by averaging the flux values at the beginning and end of the interval, then  
 291 multiplying by the interval duration. These areas are then summed to obtain the total daily  
 292 flux. This method ensures that even with some missing data points, a reliable estimate of the  
 293 daily flux can be obtained. All post-processing and statistical analyses were performed in R  
 294 4.3.2 (R Core Team, 2024) including the packages *ggplot2*, *clifro*, *MASS*, *dismo*, *amerifluxr*,  
 295 *rmarkdown*, *geosphere*, *ggmap* and *gbm*.

296

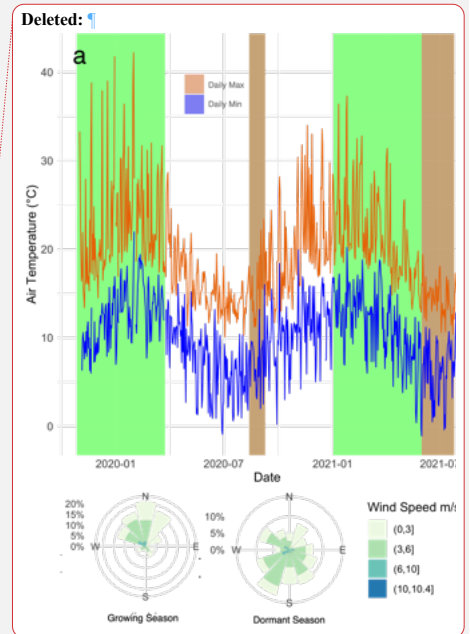
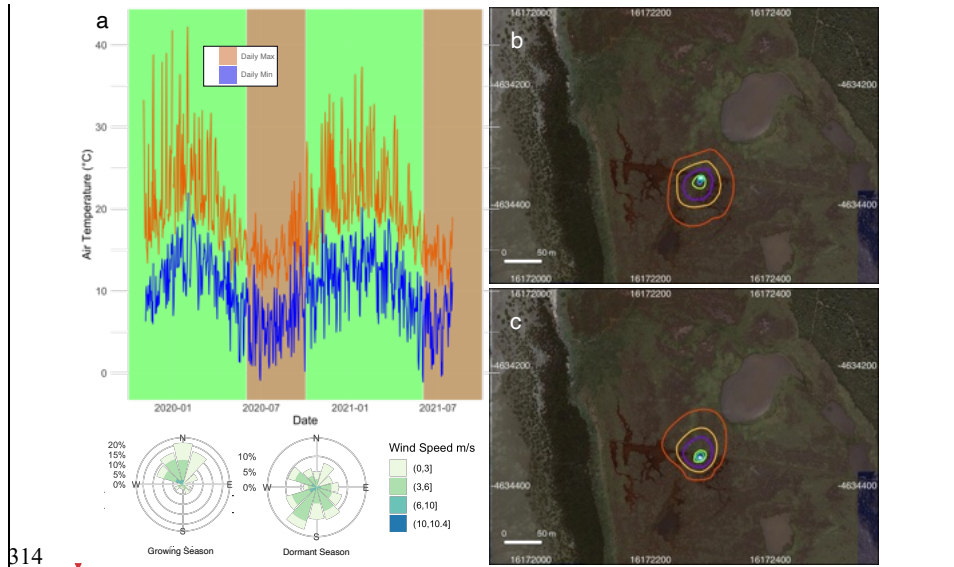
Deleted: .

298 For the CO<sub>2</sub> budget, Net Ecosystem Production (NEP), was defined as NEP=-NEE.  
 299 Nighttime NEE is referred to as R<sub>e</sub> and was corrected for temperature effects on respiration  
 300 using an exponential Arrhenius-type relationship (Lloyd and Taylor, 1994).

301  
 302 **3 Results**

303  
 304 The observations were divided into a growing season and a dormant season to reflect the  
 305 seasonal phenology of the dominant vegetation type within the flux tower footprint. During  
 306 the growing season, mean temperature averaged 22.3°C. Several heatwaves occurred during  
 307 this period, with temperatures exceeding 40°C on a few occasions in 2019. The dormant  
 308 season was significantly colder and windier, with frequent southerly winds (Fig. 2a).  
 309 Footprint models showed a slight variation in flux source between the two seasons, although  
 310 in both cases the size of the footprint and the vegetation composition within the footprint was  
 311 similar (Figs. 2b and 2c), but the shape was skewed to the north during winter due to the  
 312 prevalent southerly winds in that season (Fig. 2a). 70% of the flux measurement source was  
 313 from within 50 m of the tower, while the maximum length of the source location was 73 m.

- Moved (insertion) [1]
- Deleted: Because of the large data gaps, it was not possible
- Deleted: model the partition of the NEE in GEP and
- Deleted: using common partitioning methods (Lasslop et al., 2010). For simplicity, it was assumed that NEE at night coincided with R<sub>e</sub>.
- Formatted: Subscript
- Deleted: a linear slope of the
- Deleted: between nighttime NEE
- Deleted: temperature.
- Moved up [1]: For the CO<sub>2</sub> budget, Net Ecosystem Production (NEP), was defined as NEP=-NEE.
- Deleted: ¶
- Formatted: Outline numbered + Level: 1 + Numbering Style: 1, 2, 3, ... + Start at: 2 + Alignment: Left + Aligned at: 0 cm + Indent at: 0.63 cm
- Deleted: , which has a relatively short growing season during the summer.



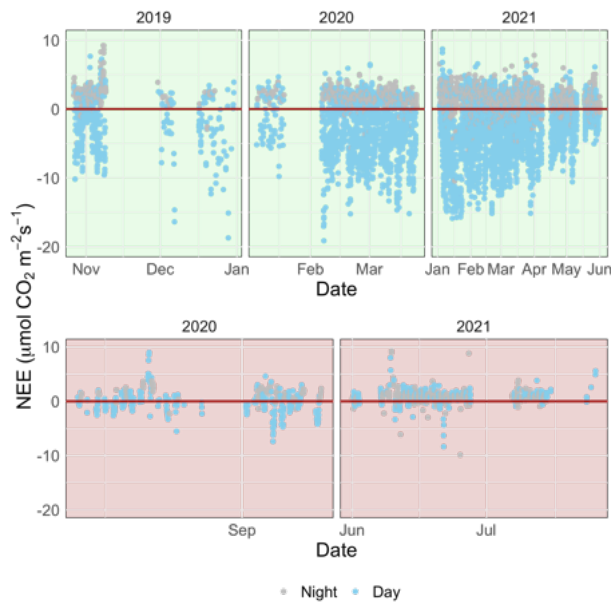
314  
 315  
 316

333 Figure 2: a) The minimum and maximum daily temperature recorded at the Cerberus  
334 meteorological station (Bureau of Meteorology, Fig. 1b) during 2019-2021. The marsh  
335 growing (October-May) and dormant (June-September) periods are shaded in green and pink  
336 respectively. A corresponding wind rose diagram summarises the wind speeds and directions  
337 measured at the tower site during the observation periods. The flux source footprint  
338 surrounding the tower during the dormant season (b) and the growing season (c) shows the  
339 cumulative flux source contribution to the flux measurements, with the outer red line  
340 representing the distance by which 90% of the calculated flux is sourced and the other  
341 isolines from the tower outwards correspond to 10%, 20%, 40%, 60% and 80% of the flux.

342  
343 The growing season dataset included 90 days with 85% or more flux data coverage, while the  
344 dormant season dataset included 18 days. There was a strong temporal variability in net  
345 ecosystem exchange (NEE) across both short (daily) and long (seasonal) temporal scales  
346 (Fig. 3). Daytime fluxes were defined as flux points where the global radiation values in the  
347 flux averaging half-hour interval were  $>12 \text{ W m}^{-2}$  (as per EddyPro methodology). At the  
348 diurnal scale, saltmarsh NEE were negative mostly during the day and positive mostly during  
349 the night and ranged between  $-19.1$  and  $10.86 \mu\text{mol m}^{-2} \text{ s}^{-1}$  across the measurement periods.  
350 Monthly averages and data coverage are shown in Table 1.

Deleted: observed during this study

352



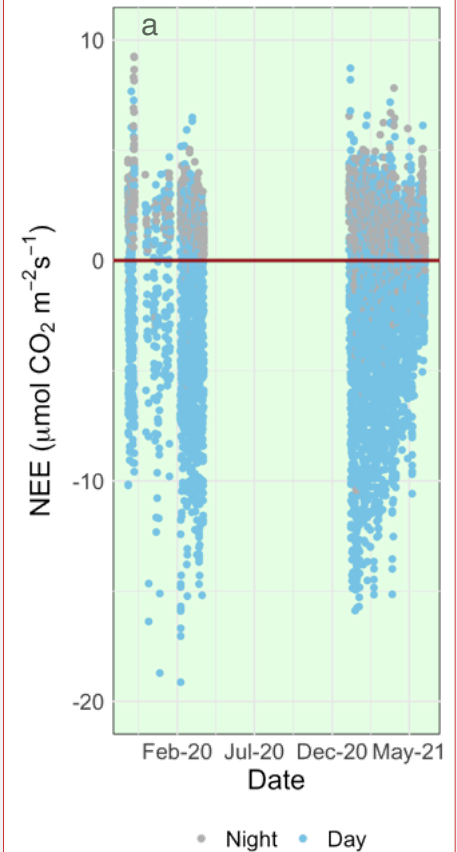
353

354 Figure 3: A time series of half-hourly measurements of CO<sub>2</sub> flux between a temperate  
355 saltmarsh and the atmosphere measured by eddy covariance during the marsh growing season  
356 (top) and the dormant season (bottom). Blue and grey points indicate measurements taken  
357 during daytime and nighttime respectively. Positive fluxes indicate a direction of flux from  
358 the Earth surface to the atmosphere.

359

360 Flux rates varied across the day, with CO<sub>2</sub> uptake peaking at 11:00 during the growing  
361 season, and later in the day (14:00) during the dormant period (Fig. 4). Ecosystem respiration  
362 rates ( $R_e$ , defined as nighttime CO<sub>2</sub> flux) were on average ( $\pm$ SD)  $1.77 (\pm 1.12) \mu\text{mol m}^{-2} \text{s}^{-1}$   
363 during the growing season and  $1.0 (\pm 0.93) \mu\text{mol m}^{-2} \text{s}^{-1}$  during the dormant period. The  
364 difference in ecosystem respiration between the growing and dormant seasons is highly  
365 significant (t-test,  $p < 0.01$ ). Daytime CO<sub>2</sub> flux was on average ( $\pm$ SD)  $-3.53 (\pm 4.15) \mu\text{mol m}^{-2}$   
366  $\text{s}^{-1}$  during the growing season and  $-0.25 (\pm 2.18) \mu\text{mol m}^{-2} \text{s}^{-1}$  during the dormant season.  
367 Thus, we derive that the maximum Gross Primary Productivity (GPP) of this ecosystem from  
368 NEE and temperature-corrected  $R_e$  (Fig. 5), measured during the growing season, is ca.  $-5.34$   
369  $\pm 4.3 \mu\text{mol CO}_2 \text{ m}^{-2} \text{ s}^{-1}$  ( $-5.53 \pm 4.45 \text{ g C m}^{-2} \text{ day}^{-1}$ ). Average  $R_e$  is thus estimated to comprise  
370 33% of GPP.

Deleted: ¶



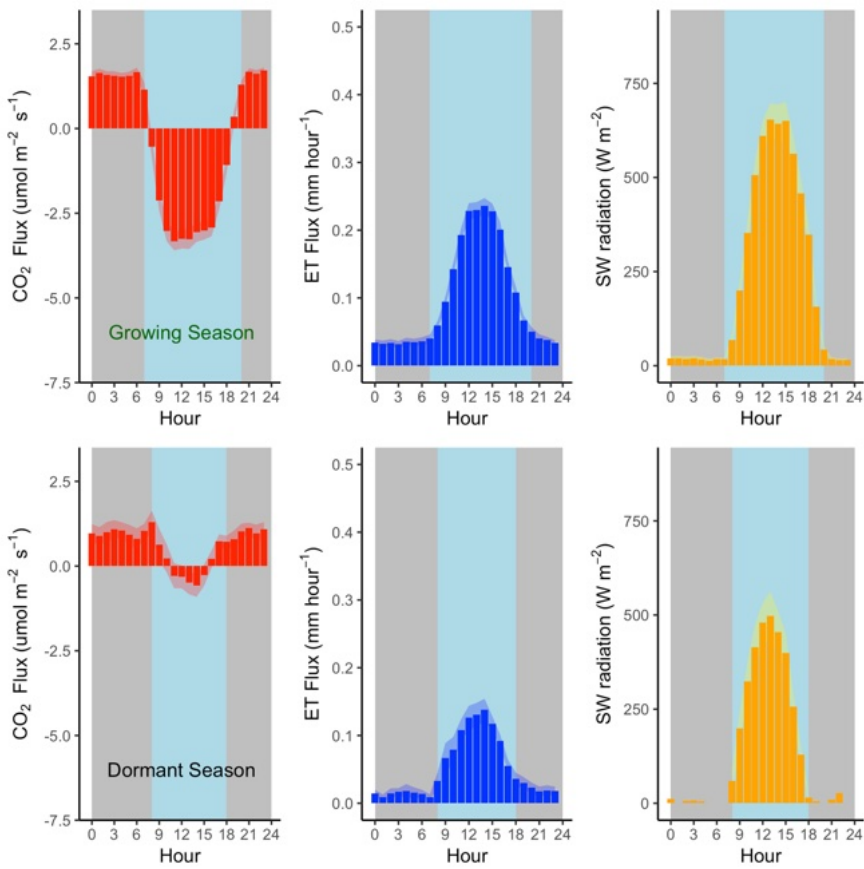
Deleted: a

Deleted: b

376

377 Mean ( $\pm$ SD) daily evapotranspiration was 2.48 mm ( $\pm$ 2.79 mm) during the growing season  
378 and 0.97 mm ( $\pm$ 1.35 mm) during the dormant season (Fig. 4). Evapotranspiration peaked at  
379 noon AEST during the growing season (0.26 mm h<sup>-1</sup>), and later in the day (14:00 AEST)  
380 during the dormant season (0.14 mm h<sup>-1</sup>).

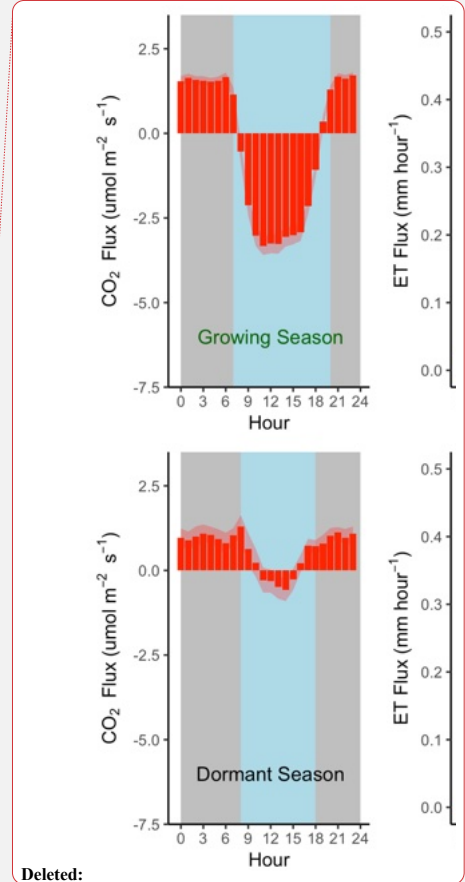
381



382

383

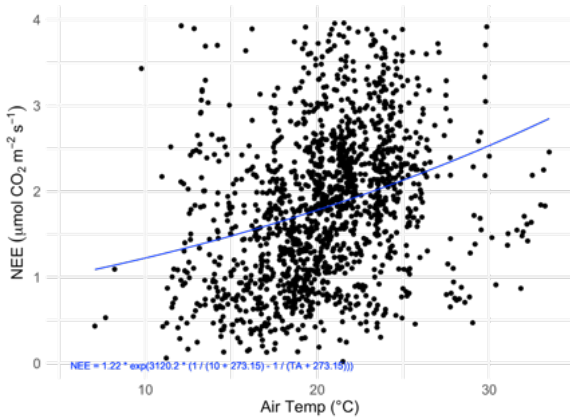
384 Figure 4: Mean hourly CO<sub>2</sub> and H<sub>2</sub>O flux (evapotranspiration) rates during the growing  
385 season (top) and the dormant season (bottom) alongside mean short wave incoming radiation.  
386 Shading corresponds to 1 standard deviation (SD) around the mean. Grey plot background



Deleted:

388 approximates nighttime periods, while light blue approximates daytime (actual day length  
389 varies within each season).

390



391

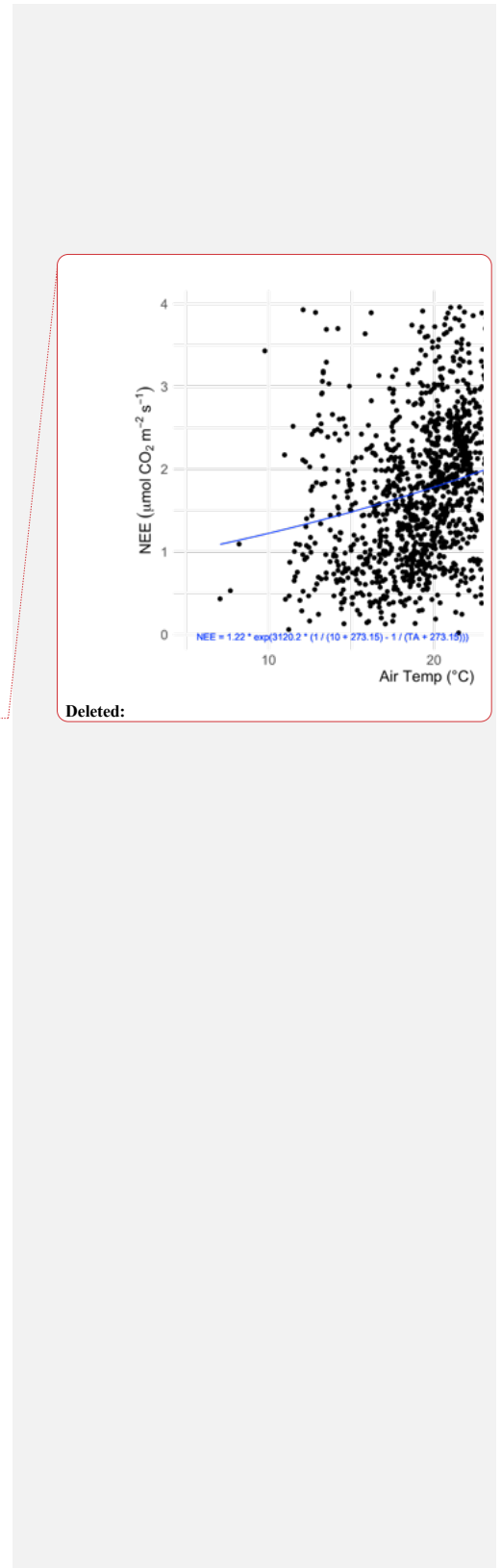
392 Figure 5: The relationship between nighttime half-hourly flux measurements (NEE) taken  
393 between the hours of 22:00 and 02:00 and air temperature (TA). The fitted curve (blue line) is  
394 the fitted Lloyd & Taylor Arrhenius non-linear model:  $NEE = 1.22 * \exp(3120.2 * (1 / 283.2 -$   
395  $1 / (TA + 273.2)))$ ,  $R^2 = 0.09$ .

396

397 The effect of some environmental forcings on daytime NEE during the saltmarsh growing  
398 season were explored (Fig. 6). To distinguish this daytime-only value from the 24-hour  
399 carbon balance integration, and to better highlight CO<sub>2</sub> uptake, NEP values are shown.

400

401 Short wave radiation (visible light) was a limiting factor to NEP below approximately 300 W  
402 m<sup>-2</sup>, but radiation did not reach damaging levels that would lead to a drop in NEP throughout  
403 the measurement range, which reached a maximum level of ca. 800 W m<sup>-2</sup>. Unlike light, the  
404 NEP-air temperature relationship followed a Gaussian response, with the highest NEP  
405 achieved at the optimal temperature of 25.3°C with a SD of 3.8°C followed by a decline in  
406 CO<sub>2</sub> uptake by the marsh at higher temperatures. The minimum and maximum air  
407 temperatures for which modelled NEP nears zero (defined here as 3 SDs from the mean) are  
408 13.9°C and 36.7°C respectively. Temperature also had a slight but significant positive linear



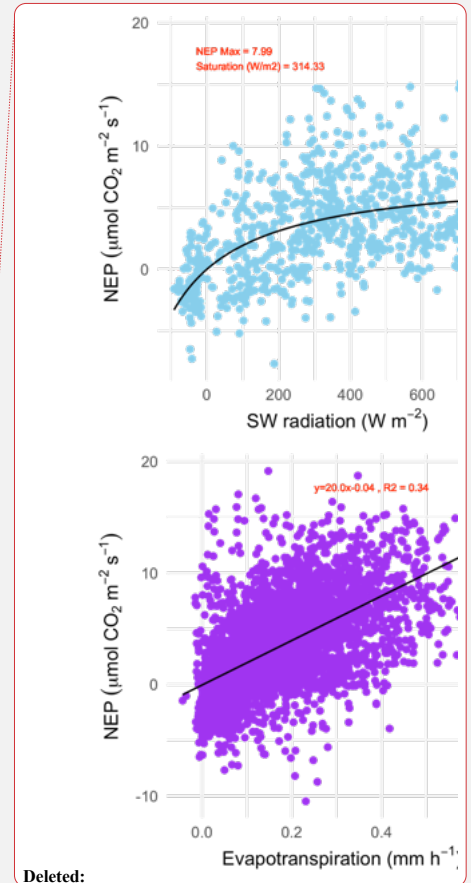
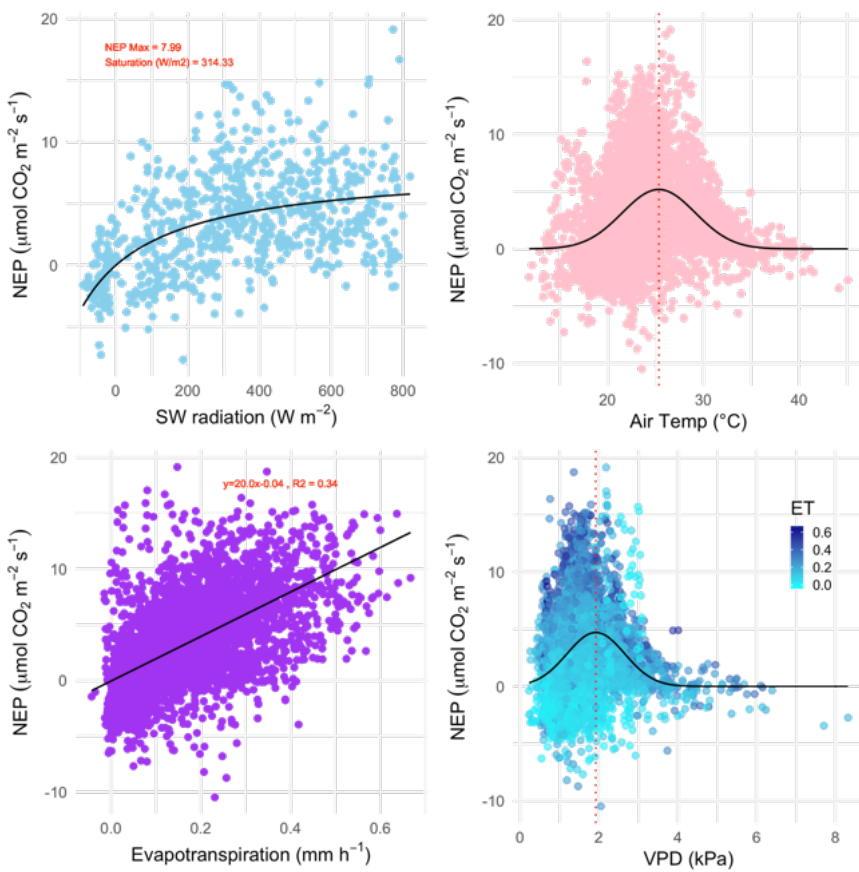
410 relationship with ecosystem respiration (slope=0.07  $\mu\text{mol CO}_2 \text{ m}^{-2} \text{ s}^{-1} \text{ }^\circ\text{C}^{-1}$ ,  $p < 0.01$ , data not  
411 shown).

412

413 NEP was positively correlated with evapotranspiration during the growing season (Pearson  $r$   
414 = 0.59, Fig.6 C). The slope of the NEP/ET relationship was 20.0, indicating an ecosystem  
415 water use efficiency ( $\text{WUE}_e$ ) of 0.86  $\text{g C kg}^{-1} \text{ H}_2\text{O}$  ( $R^2 = 0.34$ ,  $p < 0.001$ ). The response of  
416 NEP to atmospheric vapour pressure deficit (VPD) fit a Gaussian relationship (the commonly  
417 observed inverse U-shaped curve relationship in response to VPD in plants), with NEP  
418 declining rapidly when VPD exceeded 2.39 kPa. The optimal range of VPD within which  
419 NEP was maximised in this ecosystem was 1.92 kPa ( $\pm 0.73$  kPa).

420

421



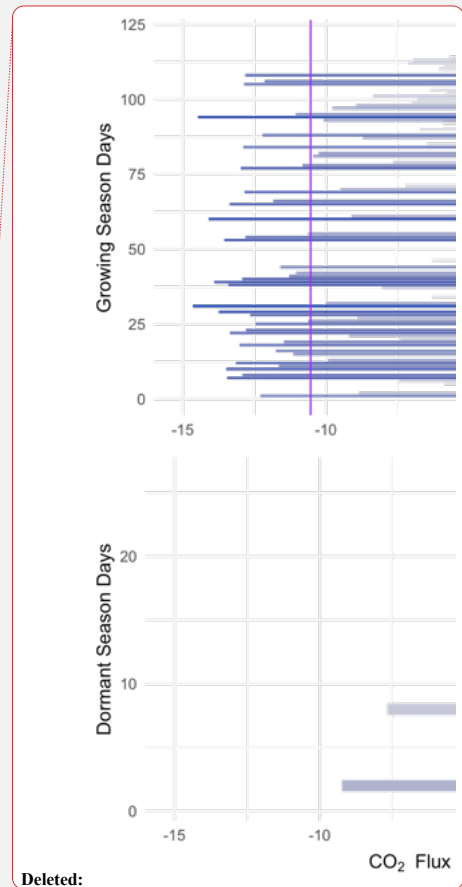
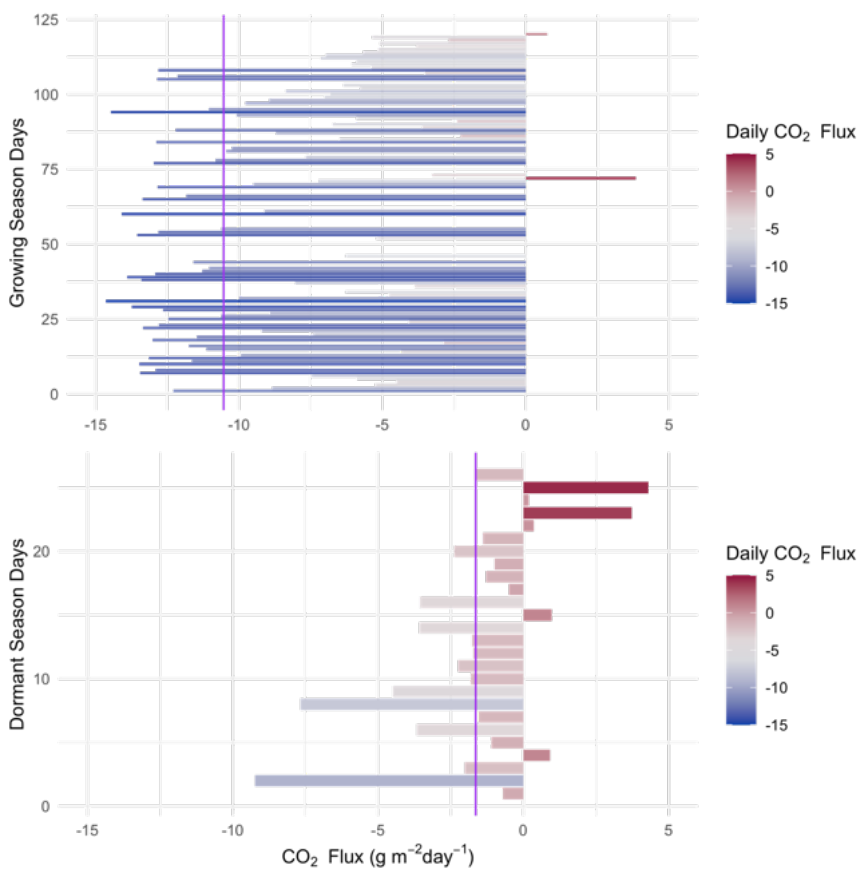


423 Figure 6: The relationship between growing season daytime half-hourly values of net  
424 ecosystem productivity (NEP,  $\mu\text{mol CO}_2 \text{ m}^{-2} \text{ s}^{-1}$ ) and corresponding environmental variables.  
425 a) Net shortwave (SW) radiation (visible light); black line is the Michaelis-Menten model of  
426 best fit. The coefficient of saturation is at  $314 \text{ W m}^{-2}$  and maximum net productivity is  $8.0$   
427  $\mu\text{mol CO}_2 \text{ m}^{-2} \text{ s}^{-1}$ . b) Air temperature, (TA); black line is a Gaussian model of best fit with a  
428 temperature optimum at  $25.3^\circ\text{C}$ . c) Evapotranspiration; linear model ( $R^2 = 0.34$ ) has a slope  
429 of  $20.0$ . d) Vapour Pressure Deficit; black line is a Gaussian model of best fit with a VPD  
430 optimum at  $1.92 \text{ kPa}$ , points are coloured by the level of evapotranspiration during the half  
431 hourly NEP measurement.

432  
433 When integrated over a 24-hour period, the saltmarsh is on average a daily  $\text{CO}_2$  sink during  
434 all canopy phenological phases (Fig. 7), although during the dormant season the sink is  
435 weaker, with an average uptake of  $-2.42 \text{ g CO}_2 \text{ m}^{-2} \text{ day}^{-1}$  ( $\pm 2.54$ ). During the growing season  
436 (defined as the non-dormant period and thus reflecting several phenological stages), the  
437 marsh is a substantial sink with a mean ( $\pm\text{SD}$ ) daily NEP of  $10.95 \text{ g CO}_2 \text{ m}^{-2} \text{ day}^{-1}$  ( $\pm 4.98$ )  
438 over a 24-hour period (ranging between  $-22.8$  and  $4.3 \text{ g}$  of  $\text{CO}_2$  emission to the atmosphere  
439  $\text{m}^{-2} \text{ day}^{-1}$ ). The daily  $\text{CO}_2$  budget during the growing season showed some variability among  
440 days ( $\text{CV}=0.46$ , Fig. 7) and days with lower average light levels (i.e. cloudy days) had a  
441 significant negative impact on the  $\text{CO}_2$  budget (multiple linear regression,  $p < 0.02$ ,  $R^2 =$   
442  $0.27$ ). Daily maximum air temperatures did not have a significant impact on the daily  $\text{CO}_2$   
443 budget ( $p = 0.77$ ) at this location, although NEE was significantly affected by temperature at  
444 finer temporal scales (Figure 6).

445  
446

Deleted: ;



Deleted:

448  
 449 Figure 7: Daily (24 h) integrated NEE in  $\text{g CO}_2 \text{ m}^{-2} \text{ day}^{-1}$  during the saltmarsh growing  
 450 season (top) and the dormant season (bottom) for days with data density  $> 85\%$ . Purple lines  
 451 indicate the mean daily integrated flux for each season ( $-10.54$  and  $-1.64 \text{ g CO}_2 \text{ m}^{-2} \text{ day}^{-1}$  with  
 452 an SD of  $4.98$  and  $2.54$  for growing and dormant respectively). A positive balance indicates  
 453 an integrated net flux of  $\text{CO}_2$  from the Earth's surface to the atmosphere over the 24-hour  
 454 period.

457 4 Discussion

458

Formatted: Outline numbered + Level: 1 + Numbering  
 Style: 1, 2, 3, ... + Start at: 2 + Alignment: Left + Aligned at:  
 0 cm + Indent at: 0.63 cm

460 The study provided high-frequency measurements of an abundant greenhouse gas (CO<sub>2</sub>)  
461 using a precise technique (eddy covariance flux) in an ecosystem with limited historical  
462 measurements. Time series analysis was performed on CO<sub>2</sub> flux measurements across various  
463 scales (daily, nightly, diel, half-hourly, hourly, seasonally) to assess the impacts of ET, SW  
464 radiation, VPD, and TA on CO<sub>2</sub> flux and how these relationships change throughout the year.

Deleted: Rad

Deleted: Tair

465 Seasonality was observed for the first time in an Australian saltmarsh and had a significant  
466 effect on carbon and water flux. Growing season net ecosystem productivity was five times  
467 greater than during the dormant period. Seasonality in Australian marshes has not been  
468 previously reported in the scientific literature and contradicts previous assumptions that  
469 Australian saltmarshes do not exhibit the growing and dormant phenology observed on other  
470 continents (Clarke and Jacoby, 1994). Seasonality had a significant impact on the daily  
471 carbon fluxes in this marsh and is an important characteristic of this habitat that has been  
472 overlooked (Owers et al., 2018). Seasonality can also have other broader implications yet to  
473 be considered in Australian marshes. For example, in the USA, the saltmarsh greening up  
474 period was shown to be an important range-wide timing event for migratory birds (Smith et  
475 al., 2020) with plant-growth metrics predicting the timing of nest initiation for shorebirds.  
476 Saltmarshes in Australia are important roosting and feeding sites along the East Asian  
477 Australasian Flyway, particularly for waders, thus potentially a similar relationship between  
478 migration timing and saltmarsh phenology could be occurring. Seasonality also affects other  
479 significant ecosystem functions such as the bio-geomorphological feedback between  
480 saltmarshes, coastal hydrodynamics and landscape evolution (Reents et al., 2022).

Deleted: budget

481  
482 We derived the light-response and associated coefficients of light regulation of saltmarsh  
483 NEE using the Michaelis-Menten model (Chen et al., 2002). Quantum (or production)  
484 efficiency is the predominant input in remote sensing techniques to model productivity, and is  
485 specific to the biome (Hilker et al., 2010). While not directly comparable to leaf level  
486 quantum efficiency measurements, the quantum efficiency ( $\alpha$ ) of the NEP light response  
487 curve was estimated from the slope of the Michaelis-Menten model to be 0.025  $\mu\text{mol CO}_2 \text{ J}^{-1}$ .  
488 The ecosystem reached light saturation at an insolation of 314  $\text{W m}^{-2}$ , but daytime insolation  
489 was below this value more than 50% of the time suggesting that light might be a significant  
490 limiting factor to NEP at this marsh, especially during winter. The level of light limitation we  
491 observed is an underestimation, due to the loss of high-quality EC data during periods of rain.  
492 The solar geometry at this latitude and the length of day result in an annual average top of

496 atmosphere SW radiation of  $250 \text{ W m}^{-2}$ , but clouds can strongly modulate the SW radiation  
497 balance (SWCRE), and apart from the months of January and February when cloudy days are  
498 less frequent (10-12 days per month), cloudy days are frequent at this site, averaging 15-17  
499 days per month (Bureau of Meteorology) and could significantly impact on NEP.

500

501 Temperature is another forcing that significantly impacts NEE at this marsh, with an optimal  
502 range for maximum NEP at  $25.3^{\circ}\text{C}$  ( $21.5^{\circ}\text{C}$ - $29.1^{\circ}\text{C}$ ). Data for Australian saltmarshes is not  
503 available, but this optimal temperature response range is similar to that measured  
504 experimentally in a saltmarsh species in an equivalent climate zone (e.g. Georgia,  
505 (Giurgevich and Dunn, 1981)) and to the values hypothesised for the habitat from data  
506 collected along the US Atlantic Coast, (Feher et al., 2017). The long-term average maximum  
507 daytime temperature at this site is  $19.2^{\circ}\text{C}$ , which is cooler than the optimal range for NEE  
508 suggesting temperature can be a significant limiting factor to productivity, especially during  
509 the dormancy period where average monthly maximum temperatures are only  $13.7^{\circ}\text{C}$  to  
510  $16.6^{\circ}\text{C}$  (Bureau of Meteorology). During the growing season the average maximum  
511 temperatures are within the range of optimal NEE ( $20.6^{\circ}\text{C}$  to  $23.1^{\circ}\text{C}$ ), although hot days  
512 ( $>30^{\circ}\text{C}$ ) significantly depress NEE and depending on the year, can be common during  
513 summer months (averaging 2-6 days per month). Within the diversity of saltmarsh species  
514 found globally, some species have C4 photosynthetic pathways (Drake, 1989). C4  
515 photosynthesis plants often exhibit higher optimum temperature ranges ( $30$ - $35^{\circ}\text{C}$ , Berry and  
516 Björkman, 1980) than C3 photosynthesis plants ( $20$ - $25$ ), and the cooler conditions at this site  
517 could explain the absence of C4 plants from this bioregion. The parabolic relationship  
518 between NEP and air temperature and NEP and VPD suggest that higher air temperatures and  
519 VPD (which are expected with climate change) could negatively impact  $\text{CO}_2$  uptake by these  
520 coastal ecosystems. High VPD was related to lower NEP, and to a lesser extent, lower ET  
521 (Fig. 6d). However, VPD increases atmospheric demand for water, increasing the evaporation  
522 from the saturated marsh surfaces in the footprint, and this atmospheric demand could be  
523 forcing ET at high VPD rather than plant moderation via reduced transpiration, even if  
524 transpiration is reduced. Thus, despite maintained ET during VPD periods we cannot  
525 conclude a non-closure of stomata. NEP also reduced below a VPD of  $1.92 \text{ KPa}$ , but at our  
526 field site low VPD correlated with low temperatures ( $r = 0.88$ ), and low temperatures were  
527 shown to limit NEP.

528

529 In saltmarshes, evapotranspiration occurs from plant mediated transpiration but also from soil  
530 pores (which tend to be saturated), wetted leaves and open water. We observed average  
531 evaporation rates of 2.48 mm day<sup>-1</sup> during the growing season and 0.97 mm day<sup>-1</sup> during the  
532 dormant season. Actual evapotranspiration in this region modelled using the CMRSET  
533 algorithm is estimated to range between 0.6 and 3.2 mm day<sup>-1</sup> during winter and summer  
534 respectively (McVicar et al., 2022); our field measurements support the model. Overall,  
535 rainfall is in excess of the requirements for maintaining ET at this site, although deficits can  
536 develop for short periods during the growing season, when ET is higher, perhaps explaining  
537 the drier saltmarsh surface during this period. Conversely, long term rainfall excess could be  
538 contributing to the complicated hydrology at this location, where inundation is not strictly  
539 associated with tidal stage (data not shown) and our observation of long (5-day) periods of  
540 inundation during winter.

541

542 Growing season ET rates are significantly higher than those of the dormant season, partly due  
543 to the solar configuration in winter as opposed to summer, but also due to phenological  
544 changes. A big leaf model estimation of evapotranspiration from saltmarshes in New South  
545 Wales estimates ET to be highly sensitive to vegetation height, increasing by more than 1 mm  
546 day<sup>-1</sup> as vegetation height increases from 0.1 to 0.4 m (Hughes et al., 2001) and transpiration  
547 in saltmarsh plants in the cold season has been shown to account for only 20% of the annual  
548 transpiration budget (Giurgevich and Dunn, 1981) following the same pattern as the seasonal  
549 distribution of productivity.

550

551 The rate of carbon uptake per unit of water loss (WUE) is a key ecosystem characteristic,  
552 which is a result of a suite of physical and canopy physiological forcings, and has direct  
553 implications for ecosystem function and global water and carbon cycling. Mean water use  
554 efficiency (WUEe) of this saltmarsh was estimated at 0.86 g C kg<sup>-1</sup> H<sub>2</sub>O, which is markedly  
555 lower than for grass dominated saltmarshes in China (2.9 g C kg<sup>-1</sup> H<sub>2</sub>O, Xiao et al. (2013))  
556 but similar to the value for WUEe based on NEP and ET in mangroves (0.77 g C kg<sup>-1</sup> H<sub>2</sub>O,  
557 Krauss et al. (2022)), which are also C3 plants. The Chinese saltmarshes studied in Xiao et al.  
558 (2013) are dominated by *Spartina alterniflora*, a C4 perennial grass. C4 plants have higher  
559 (often double) water use efficiencies than C3 plants due to CO<sub>2</sub> concentrating mechanisms  
560 (Osborne and Freckleton, 2009). The saltmarsh at French Island includes only C3 plants, and  
561 the dominant chenopod *Sarcocornia quinqueflora* has been suspected to have higher  
562 evapotranspiration rates than saltmarsh by approx. 15% (Hughes et al., 2001), but while

563 *Sarcocornia quinqueflora* dominates at this site, the footprint is a mix of species, and the  
564 lower WUE<sub>e</sub> cannot be directly linked to the presence of *Sarcocornia quinqueflora*.  
565 Furthermore, like most wetlands, the wetland surface is a mixed composition of emergent  
566 vegetation, unsaturated soil and water bodies thus the spatial scale at which WUE<sub>e</sub> is  
567 determined encompasses both the canopy (E<sub>c</sub>) as well as any open water present in the  
568 footprint. Transpiration is predicted to account for only 55% of ET in these systems (Hughes  
569 et al., 2001), which is an E<sub>c</sub> to ET ratio similar to that of mangroves (Krauss et al., 2022) but  
570 significantly lower than terrestrial forests where more than 90% of ET can be attributed to  
571 transpiration. Thus, regional variations in WUE<sub>e</sub> can be attributed to multiple forcings that  
572 form complex spatiotemporal patterns.

573  
574 Saltmarshes are considered among the most productive ecosystems on Earth with an  
575 estimated global NEP of 634 Tg C y<sup>-1</sup> (Fagherazzi et al., 2013) and 601 634 Tg C y<sup>-1</sup>  
576 (Rosentreter et al., 2023). Productivity of southern Australian marshes was previously  
577 estimated at 0.8 kg m<sup>-2</sup> y<sup>-1</sup> by repeated measurements of above ground standing crops (Clarke  
578 and Jacoby, 1994), which if not accounting for season, equates to 2.2 g C m<sup>-2</sup> d<sup>-1</sup>. Similar  
579 studies on saltmarshes in France report lower productivity (483 g C m<sup>-2</sup> y<sup>-1</sup>, (Mayen et al.,  
580 2024)) and daily growing season rates of 1.53 g C m<sup>-2</sup> d<sup>-1</sup>, but mid-latitude saltmarsh sites in  
581 the USA and China show productivity rates of 775 g C m<sup>-2</sup> y<sup>-1</sup>, (Wang et al., 2016) and 668 g  
582 C m<sup>-2</sup> y<sup>-1</sup>, (Xiao et al., 2013) respectively. It is clear that productivity across climate zones  
583 and biogeographic regions varies widely with some studies even reporting net emissions over  
584 an annual period from some marshes and a global average estimated between 382 (Alongi,  
585 2020) and 1,585 g C m<sup>-2</sup> y<sup>-1</sup> (Chmura et al., 2003), albeit based on a small subset of studies.  
586 An analysis of GPP across latitudes in the USA show that warmer sites (including mangrove  
587 wetlands in southern USA) had significantly higher GPP than mid-latitude saltmarshes such  
588 as the one on French Island (Feagin et al., 2020). Mangroves have higher NEE than  
589 saltmarshes, estimated by Krauss et al. (2022) to average 1200 g C m<sup>-2</sup> y<sup>-1</sup>. While our data  
590 does not provide enough coverage for a long-term annual estimate of carbon flux, our daily  
591 values of an average of 2.88 g C m<sup>-2</sup> d<sup>-1</sup> during the growing season, combined with the  
592 relatively short dormant season relative to other temperate locations, suggest a high carbon  
593 sequestration rate for this ecosystem type. In another southern hemisphere study, growing  
594 season rates at an EC tower site in Argentina, are extrapolated by us to average 1.6 g C m<sup>-2</sup> d<sup>-1</sup>  
595 (Bautista et al., 2023) but in that saltmarsh, flooding reduced vegetation biomass and  
596 productivity.

597

598 The data presented here is the exchange of carbon between the land surface and the  
599 atmosphere, but saltmarshes, like other marine connected communities, exchange carbon also  
600 through dissolved carbon pathways, which can be significant (Cai, 2011). Thus, the fluxes  
601 presented here do not constitute the entire carbon budget of this ecosystem.

602

## 603 5 Conclusions

604

605 The response of the French Island saltmarsh to environmental drivers is indicative of the  
606 complex interactions determining saltmarsh productivity. The unique long-term, high-  
607 resolution record enabled us to derive temperature, VPD and light response functions, thus  
608 formulating equations that describe how climate-change sensitive parameters such as  
609 temperature, relative humidity, and cloud cover, affect CO<sub>2</sub> uptake, respiration and  
610 evapotranspiration. The marsh operated as a CO<sub>2</sub> sink throughout the various canopy  
611 phenological phases, but during the dormant period, CO<sub>2</sub> uptake was less than 25% that of  
612 the growing season. Seasonality of greenhouse gas fluxes in Australian saltmarshes is an  
613 understudied but important aspect of global carbon budgeting.

614

### 615 Competing interests

616

617 The contact author has declared that none of the authors has any competing interests.

618

### 619 Acknowledgments

620

621 The work was carried out with the permission of Parks Victoria (Permit 10008684). We thank  
622 Phil and Yuko Bock for logistic support and accommodation on French Island. We thank  
623 Leigh Burgess, Kiri Mason and Ian McHugh for technical support and the Australian OzFlux  
624 community for ongoing collaboration. This work was funded by an Australian Research  
625 Council Discovery Award to RR and ED (DP220102873) as well as a Monash University  
626 Networks of Excellence award to RR.

627

### 628 Data Availability

Formatted: Outline numbered + Level: 1 + Numbering  
Style: 1, 2, 3, ... + Start at: 2 + Alignment: Left + Aligned at:  
0 cm + Indent at: 0.63 cm

629 Data used for this analysis is available at <https://figshare.com/s/ba62aafd1a4049248a08> (note  
630 that this is a temporary private link to an embargoed dataset which will be replaced with a  
631 publicly available DOI upon publication).

632

633 Author contribution

634 RR conceptualised the study, acquired funding, prepared the manuscript, designed and  
635 carried out the field campaign, and performed the analysis. ED acquired funding, developed  
636 methodology and prepared the manuscript. AG developed methodology and prepared the  
637 manuscript. TA, EJXH, HR and MP were involved in the field investigation and  
638 administration of the project and provided edits on the manuscript.

639

640 References

641

642 Adam, P.: Saltmarsh Ecology, Cambridge University Press, 1990.

643 Adam, P.: Morecambe Bay saltmarshes: 25 years of change, in: British Saltmarshes, Forrest  
644 Text, Cardigan, UK, 81–107, 2000.

645 Adam, P.: Saltmarshes in a time of change, *Environ. Conserv.*, 29, 39–61,  
646 <https://doi.org/10.1017/S0376892902000048>, 2002.

647 Alongi, D. M.: Carbon balance in salt marsh and mangrove ecosystems: A global synthesis, *J.*  
648 *Mar. Sci. Eng.*, 8, 767, 2020.

649 Artigas, F., Shin, J. Y., Hobbie, C., Marti-Donati, A., Schäfer, K. V. R., and Pechmann, I.:  
650 Long term carbon storage potential and CO<sub>2</sub> sink strength of a restored salt marsh in New  
651 Jersey, *Agric. For. Meteorol.*, 200, 313–321, <https://doi.org/10.1016/j.agrformet.2014.09.012>,  
652 2015.

653 Baldocchi, D. D.: Assessing the eddy covariance technique for evaluating carbon dioxide  
654 exchange rates of ecosystems: past, present and future, *Glob. Change Biol.*, 9, 479–492,  
655 <https://doi.org/10.1046/j.1365-2486.2003.00629.x>, 2003.

656 [Barr, A. G., Richardson, A. D., Hollinger, D. Y., Papale, D., Arain, M. A., Black, T. A.,](#)  
657 [Bohrer, G., Dragoni, D., Fischer, M. L., Gu, L., Law, B. E., Margolis, H. A., McCaughey, J.](#)  
658 [H., Munger, J. W., Oechel, W., and Schaeffer, K.: Use of change-point detection for friction-](#)  
659 [velocity threshold evaluation in eddy-covariance studies, \*Agric. For. Meteorol.\*, 171, 31–45,](#)  
660 <https://doi.org/10.1016/j.agrformet.2012.11.023>, 2013.

661 Bautista, N. E., Gassmann, M. I. , and Pérez, C. F.: Gross primary production, ecosystem  
662 respiration, and net ecosystem production in a southeastern South American salt marsh.  
664 *Estuaries Coast*, 46, 1923-1937, <https://doi.org/10.1007/s12237-023-01224-8>, 2023.

665

Moved (insertion) [2]

Moved (insertion) [3]

Moved (insertion) [4]



- 666 Berry, J., and Björkman, O.: Photosynthetic response and adaptation to temperature in higher  
667 plants, *Ann. Rev. Plant Physiol.*, 31, 491-543,  
668 <https://doi.org/10.1146/annurev.pp.31.060180.002423>, 1980.
- 669  
670 Borges, A. V., Schiettecatte, L.-S., Abril, G., Delille, B., and Gazeau, F.: Carbon dioxide in  
671 European coastal waters, *Trace Gases Eur. Coast. Zone*, 70, 375–387,  
672 <https://doi.org/10.1016/j.ecss.2006.05.046>, 2006.
- 673 Cai, W.-J.: Estuarine and coastal ocean carbon paradox: CO<sub>2</sub> sinks or sites of terrestrial  
674 carbon incineration?, *Annu. Rev. Mar. Sci.*, 3, 123–145, [https://doi.org/10.1146/annurev-](https://doi.org/10.1146/annurev-marine-120709-142723)  
675 [marine-120709-142723](https://doi.org/10.1146/annurev-marine-120709-142723), 2011.
- 676 Chen, J., Falk, M., Euskirchen, E., Paw U, K. T., Suchanek, T. H., Ustin, S. L., Bond, B. J.,  
677 Brosofske, K. D., Phillips, N., and Bi, R.: Biophysical controls of carbon flows in three  
678 successional Douglas-fir stands based on eddy-covariance measurements, *Tree Physiol.*, 22,  
679 169–177, <https://doi.org/10.1093/treephys/22.2-3.169>, 2002.
- 680 Chmura, G. L., Anisfeld, S. C., Cahoon, D. R., and Lynch, J. C.: Global carbon sequestration  
681 in tidal, saline wetland soils, *Glob. Biogeochem. Cycles*, 17,  
682 <https://doi.org/10.1029/2002GB001917>, 2003.
- 683 Clarke, P., J. and Jacoby, C. A.: Biomass and above-ground productivity of salt-marsh plants  
684 in South-eastern Australia, *Aust. J. Mar. Freshw. Res.*, 45, 1521–1528, 1994.
- 685 Davis, K. J., Bakwin, P. S., Yi, C., Berger, B. W., Zhao, C., Teclaw, R. M., and Isebrands, J.  
686 G.: The annual cycles of CO<sub>2</sub> and H<sub>2</sub>O exchange over a northern mixed forest as observed  
687 from a very tall tower, *Glob. Change Biol.*, 9, 1241-1332, [https://doi.org/10.1046/j.1365-](https://doi.org/10.1046/j.1365-2486.2003.00672.x)  
688 [2486.2003.00672.x](https://doi.org/10.1046/j.1365-2486.2003.00672.x), 2003.
- 689 Drake, B. G.: Photosynthesis of salt marsh species, *Aquat. Bot.*, 34, 167-180,  
690 [https://doi.org/10.1016/0304-3770\(89\)90055-7](https://doi.org/10.1016/0304-3770(89)90055-7), 1989.
- 691  
692 Duarte, C. M.: Reviews and syntheses: Hidden forests, the role of vegetated coastal habitats  
693 in the ocean carbon budget, *Biogeosciences*, 14, 301–310, [https://doi.org/10.5194/bg-14-301-](https://doi.org/10.5194/bg-14-301-2017)  
694 [2017](https://doi.org/10.5194/bg-14-301-2017), 2017.
- 695 Erickson, J. E., Peresta, G., Montovan, K. J., and Drake, B. G.: Direct and indirect effects of  
696 elevated atmospheric CO<sub>2</sub> on net ecosystem production in a Chesapeake Bay tidal wetland,  
697 *Glob. Change Biol.*, 19, 3368–3378, 2013.
- 698 Fagherazzi, S., Wiberg, P. L., Temmerman, S., Struyf, E., Zhao, Y., and Raymond, P. A.:  
699 Fluxes of water, sediments, and biogeochemical compounds in salt marshes, *Ecol. Process.*,  
700 2, 3, <https://doi.org/10.1186/2192-1709-2-3>, 2013.
- 701 Feagin, R. A., Forbrich, I., Huff, T. P., Barr, J. G., Ruiz-Plancarte, J., Fuentes, J. D., Najjar,  
702 R. G., Vargas, R., Vázquez-Lule, A., Windham-Myers, L., Kroeger, K. D., Ward, E. J.,  
703 Moore, G. W., Leclerc, M., Krauss, K. W., Stagg, C. L., Alber, M., Knox, S. H., Schäfer, K.  
704 V. R., Bianchi, T. S., Hutchings, J. A., Nahrawi, H., Noormets, A., Mitra, B., Jaimes, A.,  
705 Hinson, A. L., Bergamaschi, B., King, J. S., and Miao, G.: Tidal wetland gross primary  
706 production across the continental United States, 2000–2019, *Glob. Biogeochem. Cycles*, 34,  
707 [e2019GB006349](https://doi.org/10.1029/2019GB006349), <https://doi.org/10.1029/2019GB006349>, 2020.

- 708 Feher, L. C., Osland, M. J., Griffith, K. T., Grace, J. B., Howard, R. J., Stagg, C. L.,  
 709 Enwright, N. M., Krauss, K. W., Gabler, C. A., Day, R. H., and Rogers, K.: Linear and  
 710 nonlinear effects of temperature and precipitation on ecosystem properties in tidal saline  
 711 wetlands, *Ecosphere*, 8, e01956, <https://doi.org/10.1002/ecs2.1956>, 2017.
- 712 Gedan, K. B., Silliman, B. R., and Bertness, M. D.: Centuries of human-driven change in salt  
 713 marsh ecosystems, *Annu. Rev. Mar. Sci.*, 1, 117–141,  
 714 <https://doi.org/10.1146/annurev.marine.010908.163930>, 2009.
- 715 Ghosh, S. and Mishra, D. R.: Analyzing the long-term phenological trends of salt marsh  
 716 ecosystem across coastal Louisiana, *Remote Sens.*, 9, <https://doi.org/10.3390/rs9121340>,  
 717 2017.
- 718 Giurgevich, J. R. and Dunn, E. L.: A comparative analysis of the CO<sub>2</sub> and water vapor  
 719 responses of two *Spartina* species from Georgia coastal marshes, *Estuar. Coast. Shelf Sci.*,  
 720 12, 561–568, [https://doi.org/10.1016/S0302-3524\(81\)80082-5](https://doi.org/10.1016/S0302-3524(81)80082-5), 1981.
- 721 Hilker, T., Hall, F. G., Coops, N. C., Lyapustin, A., Wang, Y., Nestic, Z., Grant, N., Black, T.  
 722 A., Wulder, M. A., Kljun, N., Hopkinson, C., and Chasmer, L.: Remote sensing of  
 723 photosynthetic light-use efficiency across two forested biomes: Spatial scaling, *Remote Sens.*  
 724 *Environ.*, 114, 2863–2874, <https://doi.org/10.1016/j.rse.2010.07.004>, 2010.
- 725 Hill, A. C. and Vargas, R.: Methane and carbon dioxide fluxes in a temperate tidal salt marsh:  
 726 comparisons between plot and ecosystem measurements, *J. Geophys. Res. Biogeosciences*,  
 727 127, e2022JG006943, <https://doi.org/10.1029/2022JG006943>, 2022.
- 728 Howe, A. J., Rodríguez, J. F., Spencer, J., MacFarlane, G. R., and Saintilan, N.: Response of  
 729 estuarine wetlands to reinstatement of tidal flows, *Mar. Freshw. Res.*, 61, 702–713, 2010.
- 730 Hughes, C. E., Kalma, J. D., Binning, P., Willgoose, G. R., and Vertzonis, M.: Estimating  
 731 evapotranspiration for a temperate salt marsh, Newcastle, Australia, *Hydrol. Process.*, 15,  
 732 957–975, <https://doi.org/10.1002/hyp.189>, 2001.
- 733 Huxham, M., Whitlock, D., Githaiga, M., and Dencer-Brown, A.: Carbon in the coastal  
 734 seascape: how interactions between mangrove forests, seagrass meadows and tidal marshes  
 735 influence carbon storage, *Curr. For. Rep.*, 4, 101–110, <https://doi.org/10.1007/s40725-018-0077-4>, 2018.
- 737 Kathilankal, J. C., Mozdzer, T. J., Fuentes, J. D., D’Odorico, P., McGlathery, K. J., and  
 738 Ziemann, J. C.: Tidal influences on carbon assimilation by a salt marsh, *Environ. Res. Lett.*, 3,  
 739 044010, <https://doi.org/10.1088/1748-9326/3/4/044010>, 2008.
- 740 Kljun, N., Calanca, P., Rotach, M. W., and Schmid, H. P.: A simple two-dimensional  
 741 parameterisation for Flux Footprint Prediction (FFP), *Geosci Model Dev*, 8, 3695–3713,  
 742 <https://doi.org/10.5194/gmd-8-3695-2015>, 2015.
- 743 Krauss, K. W., Lovelock, C. E., Chen, L., Berger, U., Ball, M. C., Reef, R., Peters, R.,  
 744 Bowen, H., Vovides, A. G., Ward, E. J., and others: Mangroves provide blue carbon  
 745 ecological value at a low freshwater cost, *Sci. Rep.*, 12, <https://doi.org/10.1038/s41598-022-11111-1>, 2022.
- 746 Lloyd, J., and Taylor, J. A.: On the temperature dependence of soil respiration, *Funct. Ecol.*,  
 747 8(3), 315–323. <https://doi.org/10.2307/2389824>, 1994.

Deleted: Lasslop,

749  
750 Lu, W., Xiao, J., Liu, F., Zhang, Y., Liu, C., and Lin, G.: Contrasting ecosystem CO<sub>2</sub> fluxes  
751 of inland and coastal wetlands: a meta-analysis of eddy covariance data, *Glob. Change Biol.*,  
752 23, 1180–1198, <https://doi.org/10.1111/gcb.13424>, 2017.

753 Mayen, J., Polsenaere, P., Lamaud, É., Arnaud, M., Kostyrka, P., Bonnefond, J.-M., Geairon,  
754 P., Gernigon, J., Chassagne, R., and Lacoue-Labarthe, T.: Atmospheric CO<sub>2</sub> exchanges  
755 measured by eddy covariance over a temperate salt marsh and influence of environmental  
756 controlling factors, *Biogeosciences*, 21, 993–1016, 2024.

757 McLeod, E., Chmura, G. L., Bouillon, S., Salm, R., Björk, M., Duarte, C. M., Lovelock, C.  
758 E., Schlesinger, W. H., and Silliman, B. R.: A blueprint for blue carbon: toward an improved  
759 understanding of the role of vegetated coastal habitats in sequestering CO<sub>2</sub>, *Front. Ecol.*  
760 *Environ.*, 9, 552–560, <https://doi.org/10.1890/110004>, 2011.

761 Mcowen, C. J., Weatherdon, L. V., Bochove, J.-W. V., Sullivan, E., Blyth, S., Zockler, C.,  
762 Stanwell-Smith, D., Kingston, N., Martin, C. S., Spalding, M., and Fletcher, S.: A global map  
763 of saltmarshes, *Biodivers. Data J.*, 5, e11764, <https://doi.org/10.3897/BDJ.5.e11764>, 2017.

764 McVicar, T., Vleeshouwer, J., Van Niel, T., Guerschman, J., and Peña-Arancibia, J. L.:  
765 Actual Evapotranspiration for Australia using CMRSET algorithm. Version 1.0, 2022.

766 Mitsch, W. J. and Gosselink, J. G.: The value of wetlands: importance of scale and landscape  
767 setting, *Ecol. Econ.*, 35, 25–33, [https://doi.org/10.1016/S0921-8009\(00\)00165-8](https://doi.org/10.1016/S0921-8009(00)00165-8), 2000.

768 Moffett, K. B., Wolf, A., Berry, J. A., and Gorelick, S. M.: Salt marsh–atmosphere exchange  
769 of energy, water vapor, and carbon dioxide: Effects of tidal flooding and biophysical controls,  
770 *Water Resour. Res.*, 46, 2010.

771 Nahrawi, H., Leclerc, M. Y., Pennings, S., Zhang, G., Singh, N., and Pahari, R.: Impact of  
772 tidal inundation on the net ecosystem exchange in daytime conditions in a salt marsh, *Agric.*  
773 *For. Meteorol.*, 294, 108133, <https://doi.org/10.1016/j.agrformet.2020.108133>, 2020.

774 Navarro, A., Young, M., Macreadie, P. I., Nicholson, E., and Ierodiaconou, D.: Mangrove  
775 and saltmarsh distribution mapping and land cover change assessment for south-eastern  
776 Australia from 1991 to 2015, *Remote Sens.*, 13, <https://doi.org/10.3390/rs13081450>, 2021.

777 Osborne, C. P. and Freckleton, R. P.: Ecological selection pressures for C4 photosynthesis in  
778 the grasses. *Proc. Roc. Soc. B*, 276, <https://doi.org/10.1098/rspb.2008.1762>, 2009.

779 Otani, S. and Endo, T.: CO<sub>2</sub> flux in tidal flats and salt marshes, *Blue Carbon Shallow Coast.*  
780 *Ecosyst. Carbon Dyn. Policy Implement.*, 223–250, 2019.

781 Owers, C. J., Rogers, K. and Woodroffe, C. D.: Spatial variation of above-ground carbon  
782 storage in temperate coastal wetlands. *Estuar. Coast. Shelf Sci.*, 210, 55–67,  
783 <https://doi.org/10.1016/j.ecss.2018.06.002>, 2018

784  
785 R Core Team: R: A Language Environment for Statistical Computing. Vienna, Australia,  
786 2024.

787 Reents, S., Möller, I., Evans, B. R., Schoutens, K., Jensen, K., Paul, M., Bouma, T. J.,  
788 Temmerman, S., Lustig, J., Kudella, M., and Nolte, S.: Species-specific and seasonal

Moved up [2]: G.,  
Moved up [3]: Richardson, A. D.,  
Moved up [4]: A.,  
Deleted: Reichstein, M., Papale, D.,  
Deleted: Arneeth, A., BARR,  
Deleted: STOY, P., and WOHLFAHRT, G.: Separation of net ecosystem exchange into assimilation and respiration using a light response curve approach: critical issues and global evaluation, *Glob. Change Biol.*, 16, 187–208, <https://doi.org/10.1111/j.1365-2486.2009.02041.x>, 2010.  
Formatted: Normal

799 differences in the resistance of salt-marsh vegetation to wave impact, *Front. Mar. Sci.*, 9,  
800 2022.

801 Rosentreter, J. A., Laruelle, G. G., Bange, H. W., Bianchi, T. S., Busecke, J. J. M., Cai, W. J.,  
802 Eyre, B. D., Forbich, I., Kwon, E. Y., Maavara, T., Moosdorf, N., Najjar, R. G., Sarma, V. V.  
803 S. S., Van Dam, B. and Regnier, P.: Coastal vegetation and estuaries are collectively a  
804 greenhouse gas sink. *Nat. Clim. Chang.* 13, 579–587. [https://doi.org/10.1038/s41558-023-](https://doi.org/10.1038/s41558-023-01682-9)  
805 [01682-9](https://doi.org/10.1038/s41558-023-01682-9), 2023.

806  
807 Schäfer, K. V. R., Duman, T., Tomasicchio, K., Tripathee, R., and Sturtevant, C.: Carbon  
808 dioxide fluxes of temperate urban wetlands with different restoration history, *Agric. For.*  
809 *Meteorol.*, 275, 223–232, <https://doi.org/10.1016/j.agrformet.2019.05.026>, 2019.

810 Seyfferth, A. L., Bothfeld, F., Vargas, R., Stuckey, J. W., Wang, J., Kearns, K., Michael, H.  
811 A., Guimond, J., Yu, X., and Sparks, D. L.: Spatial and temporal heterogeneity of  
812 geochemical controls on carbon cycling in a tidal salt marsh, *Geochim. Cosmochim. Acta*,  
813 282, 1–18, 2020.

814 Shepard, C. C., Crain, C. M., and Beck, M. W.: The protective role of coastal marshes: a  
815 systematic review and meta-analysis, *PLoS ONE*, 6, e27374,  
816 <https://doi.org/10.1371/journal.pone.0027374>, 2011.

817 Smith, J. A. M., Regan, K., Cooper, N. W., Johnson, L., Olson, E., Green, A., Tash, J., Evers,  
818 D. C., and Marra, P. P.: A green wave of saltmarsh productivity predicts the timing of the  
819 annual cycle in a long-distance migratory shorebird, *Sci. Rep.*, 10, 20658,  
820 <https://doi.org/10.1038/s41598-020-77784-7>, 2020.

821 Vázquez-Lule, A. and Vargas, R.: Biophysical drivers of net ecosystem and methane  
822 exchange across phenological phases in a tidal salt marsh, *Agric. For. Meteorol.*, 300,  
823 108309, <https://doi.org/10.1016/j.agrformet.2020.108309>, 2021.

824 Wang, Z. A., Kroeger, K. D., Ganju, N. K., Gonneea, M. E., and Chu, S. N.: Intertidal salt  
825 marshes as an important source of inorganic carbon to the coastal ocean, *Limnol. Oceanogr.*,  
826 61, 1916–1931, <https://doi.org/10.1002/lno.10347>, 2016.

827 Ward, N. D., Megonigal, J. P., Bond-Lamberty, B., Bailey, V. L., Butman, D., Canuel, E. A.,  
828 Diefenderfer, H., Ganju, N. K., Goñi, M. A., and Graham, E. B.: Representing the function  
829 and sensitivity of coastal interfaces in Earth system models, *Nat. Commun.*, 11, 2458, 2020.

830 Wei, S., Han, G., Jia, X., Song, W., Chu, X., He, W., Xia, J., and Wu, H.: Tidal effects on  
831 ecosystem CO<sub>2</sub> exchange at multiple timescales in a salt marsh in the Yellow River Delta,  
832 *Estuar. Coast. Shelf Sci.*, 238, 106727, 2020.

833 Whitfield, A. K.: The role of seagrass meadows, mangrove forests, salt marshes and reed  
834 beds as nursery areas and food sources for fishes in estuaries, *Rev. Fish Biol. Fish.*, 27, 75–  
835 110, <https://doi.org/10.1007/s11160-016-9454-x>, 2017.

836 Xiao, J., Sun, G., Chen, J., Chen, H., Chen, S., Dong, G., Gao, S., Guo, H., Guo, J., Han, S.,  
837 Kato, T., Li, Y., Lin, G., Lu, W., Ma, M., McNulty, S., Shao, C., Wang, X., Xie, X., Zhang,  
838 X., Zhang, Z., Zhao, B., Zhou, G., and Zhou, J.: Carbon fluxes, evapotranspiration, and water

839 use efficiency of terrestrial ecosystems in China, *Agric. For. Meteorol.*, 182–183, 76–90,  
840 <https://doi.org/10.1016/j.agrformet.2013.08.007>, 2013.

841